Object Representation Enhancement through Intrinsic Tactile Continuous Exploration

Carlos Rosales[1], Arash Ajoudani[2], Marco Gabiccini[3] and Antonio Bicchi[4]

***Abstract*— An object representation is normally needed for object recognition and robotic grasp planning. Most of the time, the representation involves only structure-related properties of the object, namely shape and size. However, the mechanical properties are very relevant in grasp planning using robotic hands, such as the friction coefficient or the surface compliance, and they are omitted in general in previous approaches. This work proposes an object representation that comprises both the shape and the friction coefficient, as well as the exploration strategy to collect them. The representation is developed under a probabilistic framework, particularly it uses Gaussian processes, to tackle the uncertainty and noise of the sensor measurements. The exploration strategy relies on the representation to compute straight lines on the surface, called geodesic flows, to ensure a positive information gain. The actual exploration follows the computed paths by employing an stiffness controller in pursuance of safety, shape accommodation and contact constraint. The procedure makes use of an RGB-D camera and an Intrinsic Tactile sensor (ITS) mounted on a robotic arm as an end-effector. The proposed exploration strategy is applied to different object shapes and materials in a real robotic platform. Experimental results give evidence for the effectiveness of the algorithm in enrichment of the object representation.**

I. INTRODUCTION

Objects are perceived by robotic systems using non-contact or contact sensing, or a combination of both, for essential tasks such as recognition and grasping and manipulation. Non-contact sensing includes the use of stereo-vision, and more recently RGB-D cameras, but not limited to, and has received more attention than its counterpart the contact sensing, perhaps due to the fact that the latter are usually built for a specific hardware. Contact sensors mainly include pressure sensor arrays (also known as tactile arrays) and Intrinsic Tactile sensors (ITs), that we shall detail later. Visual and tactile array information has been successfully integrated using object shape representations for different purposes. For instance, [1] uses the tactile information to discriminate object pose hypothesis coming from vision, [2] defines a hierarchical strategy to explore the object using the tactile information to refine the object shape only when necessary. In more recent works, [3] fuses the two sources of information by applying symmetry constraints to reconstruct the complete object shape, and [4] uses the contact points to improve the object pose within the hand, initially obtained by vision. Nonetheless, other object properties apart from the shape are hardly explored, perhaps due to the fact that one needs specific sensory systems to measure them in addition to a proper representation to process the information. In this preliminary work, the hardware setup we present resembles those of pioneers works [5] and [6] (see Fig. 1), but instead of using tactile arrays at tip of the exploratory probe, we use an ITs because of its capability to retrieve the contact force [7], which is crucial to our approach. However, the testbed for the complete pipeline to be developed in the future is to use a dexterous hand equipped with ITs at the fingertip for active in-hand exploration (Fig. 1, top).

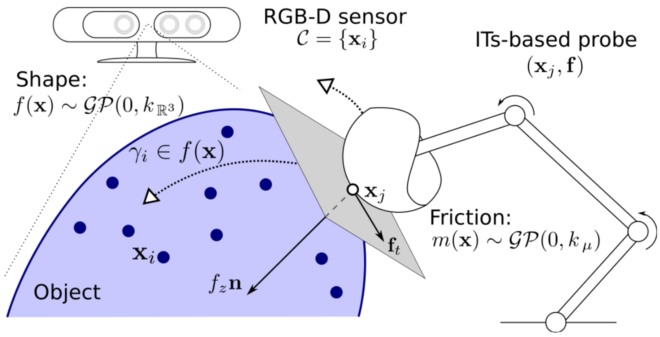

Fig. 1: The shape is acquired by an RGB-D sensor and the friction coefficient by the intrinsic tactile sensor, both shape $f(\mathbf{x})$ and friction $m(\mathbf{x})$ are represented as a Gaussian process $\mathcal{GP}(0, k(\cdot))$. The exploration follows geodesic flows γ_i on the surface using a compliant behavior.

This work proposes a methodology to enhance the object representation by adding a mechanical-related object property: the friction coefficient; a potential feature for object recognition [8], and certainly relevant to grasp determination [9], as well as the exploration strategy to collect it. The representation is developed under a probabilistic framework, particularly it uses Gaussian processes (GPs), which has proved to provide good results in object recognition [10] and object grasping [11], [12]. Thus, the shape is approximated by a Gaussian process over the object point cloud captured by an RGB-D sensor. Regarding the haptic exploration strategy,

[1] C. Rosales is with Centro di Ricerca "E. Piaggio", Università di Pisa, 1 Largo L. Lazzarino, 56122 Pisa, Italy. {carlos.rosales} at for.unipi.it

[2] A. Ajoudani is with the Department of Advanced Robotics (ADVR), Istituto Italiano di Tecnologia, Genova, Italy {arash.ajoudani} at iit.it

[3] M. Gabiccini is with the Centro di Ricerca "E. Piaggio", Università di Pisa, 1 Largo L. Lazzarino, 56122 Pisa, Department of Civil and Industrial Engineering (DICI), Largo Lucio Lazzarino 1, Pisa and Department of Advanced Robotics (ADVR), Italian Institute of Technology, 30 Via Morego, 16163 Genova, Italy. m.gabiccini at ing.unipi.it

[4] A. Bicchi is with the Centro di Ricerca "E. Piaggio", Università di Pisa, 1 Largo L. Lazzarino, 56122 Pisa and Department of Advanced Robotics (ADVR), Italian Institute of Technology, 30 Via Morego, 16163 Genova, Italy. bicchi at centropiaggio.unipi.it

ideally, it is desired that the ratio between the information gain and the exploration length (time or distance) be high. Since nothing is known about the object *a priori*, the best choice seems to be straight lines over the surface, here called geodesic flows. The shape representation allows the computation of such lines, here called geodesic flows. The actual exploration is executed by ITs mounted on a 7 DoF arm. To this end, a controlled compliant behavior should provide a safe contact, shape accommodation and good data quality acquisition. The friction coefficient over the explored surface is approximated by Gaussian process as well. The rest of the paper is organized as follows: Section II describes the devices and type of information they provide, Section III details the object representation and the exploration strategy, Section IV shows the experimental results, and, finally, Section V draws the conclusions and points for future developments.

II. Sensory data

As shown in Fig. 1, the setup is composed of an RGB-D sensor and an ITs mounted on a robot's end-effector. Visual and tactile data acquired from them are described below.

A. Visual data

The object surface is acquired using a commercial RGB-D sensor (Fig. 2a). The raw data comes in a point cloud format and it is pre-processed to isolate the object point cloud, $\mathcal{C} = \{\mathbf{x}_1, \ldots, \mathbf{x}_N\}$, where $\mathbf{x}_i \in \mathbb{R}^3$ is a point on the surface w.r.t. to the sensor frame. It is also possible to estimate the normal at the contact points which will be useful in the object representation learning (Subsection III-A).

B. Tactile data

The ITs is composed of a force/torque (F/T) sensor, a tip and a compliant structure as safety mechanism due to the high cost of the F/T sensor (Fig. 2b). The tactile data coming from it include the contact point on the object surface, $\mathbf{x}_j \in \mathbb{R}^3$ w.r.t. the F/T sensor frame, and the contact force $\mathbf{f}_j \in \mathbb{R}^3$ expressed in the contact frame, such that we are able to compute

$$\mu = \frac{||\mathbf{f}_t||}{||f_z||}, \tag{1}$$

where f_z and $\mathbf{f}_t$ are the components in the normal and in the tangent plane at the contact point, respectively (Fig. 1).

The tip is spherical for simplicity on the contact point calculation, but other ellipsoidal surfaces could be used as well [7]. The compliant mechanism is an in-parallel passive compliant coupler (PPCC) with known Cartesian stiffness, such that the deformation can be approximated using the F/T measurements to obtain the tactile data w.r.t. to a fixed frame. However, in our case, the ITs is mounted on a 7 DoF KUKA robotic arm to form the exploratory probe with high mobility.

(a) RGB-D sensor. (b) Intrinsic Tactile sensor.

Fig. 2: Visual and tactile devices.

III. Exploration Strategy

The proposed strategy is based on three main ingredients: object representation for a complemented sensory data processing, exploration paths for an optimal information gain, and contour following for a successful data acquisition. Details on each of them are presented next.

A. Object Representation: Gaussian processes for implicit functions

The object shape is modeled by an implicit function, $f(\mathbf{x}) = 0$, with $\mathbf{x} \in \mathbb{R}^3$ being any point on the surface. This function is approximated using a Gaussian process (GP) [13] over the object point cloud, $\mathcal{C}$, as

$$f(\mathbf{x}) \sim \sum_{i=1}^{N} \alpha_i k_{\mathbb{R}_3}(\mathbf{x}, \mathbf{x}_i, \sigma), \tag{2}$$

where $k_{\mathbb{R}_3}(\cdot)$ is the covariance function centered at points $\mathbf{x}_i \in \mathcal{C}$, σ is a smoothing parameter, it is set according to the units of $\mathbf{x}$, and it is enforced to have the same value for all terms, and α_i is the weighing factor for each term, and it is to be learned from the measurements.

For 3D points, we use a triangular position kernel (see [10], [14] for more details), which has the form

$$k_{\mathbb{R}_3}(\mathbf{d}, \sigma) = \begin{cases} 1 - \dfrac{(\mathbf{d}^\intercal \mathbf{d})^{\frac{1}{2}}}{2\sigma} & \text{if } (\mathbf{d}^\intercal \mathbf{d})^{\frac{1}{2}} \leq 2\sigma \\ 0 & \text{if } (\mathbf{d}^\intercal \mathbf{d})^{\frac{1}{2}} > 2\sigma, \end{cases} \tag{3}$$

where we perform the change of variable $\mathbf{d} = \mathbf{x} - \mathbf{x}_i, \forall i$.

The friction coefficient value over the surface is also modeled by an implicit function, $m(\mathbf{d})$, and approximated as well by a GP, as

$$m(\mathbf{d}) \sim \sum_{i=1}^{N} \beta_i k_{\mu}(\mathbf{d}, \Sigma). \tag{4}$$

Due to the nature of the data, we decide to use a squared exponential as the covariance function instead, with the form

$$k_{\mu}(\mathbf{d}, \Sigma) = e^{\frac{(\mathbf{d}^\intercal \mathbf{d})}{2\Sigma}}, \tag{5}$$

where Σ is a smoothing factor without units. It is worth noting that, the points on the surface in this case come from both the tactile and visual data (Section II).

The determination of the weights α_i and β_i depends on the function we want to represent to choose proper labels to the sensory data. In the case of the object surface, we would like to model

$$f(\mathbf{x}) \begin{cases} > 0, & \text{if } \mathbf{x} \text{ is outside the surface} \\ = 0, & \text{if } \mathbf{x} \text{ is on the surface} \\ < 0, & \text{if } \mathbf{x} \text{ is inside the surface,} \end{cases} \tag{6}$$

therefore, the labeling goes for a positive, null or zero value, e.g. 1, 0 and -1, for points that are outside, on, or inside the surface, respectively. The set containing the points on the surfaces are directly in the visual data (Subsection II-A). The set containing points outside the surface is generated by estimating the outward normal over the previous set, and then, displacing the points along the normal. The set containing points inside could be created using a similar method, however, only one inside the surface proved to be enough. Thus, let the vector $\mathbf{y} = (y_1, \ldots, y_i, \ldots, y_s)^\mathsf{T}$ contains the labels corresponding to the joined point set, and covariance matrix $K_{\mathbb{R}_3}$ with elements $k_{ij,\mathbb{R}_3} = k_{\mathbb{R}_3}(\mathbf{d}_{ij}, \sigma)$, with $\mathbf{d}_{ij} = \mathbf{x}_i - \mathbf{x}_j$ for all points, the weights are approximated under simplifying assumptions as

$$(\alpha_1, \ldots, \alpha_i, \ldots, \alpha_N)^\mathsf{T} = K_{\mathbb{R}_3}^{-1}\mathbf{y}. \tag{7}$$

In the case of the friction coefficient function, we would like to model

$$m(\mathbf{x}) \begin{cases} = \mu, & \text{if } \mathbf{x} \text{ is on the surface} \\ < 0, & \text{otherwise,} \end{cases} \tag{8}$$

therefore, the labels are the estimated friction coefficient and negative, e.g. -1, for points from the tactile and visual data, respectively. Note that, a non-sense value for the friction coefficient is assigned for points that are not explored yet but are known to be on the surface. Like so, the weights are approximated again by arranging a proper label vector $\mathbf{n} = (n_1, \ldots, n_i, \ldots, n_N)^\mathsf{T}$ and covariance matrix K_μ with elements $k_{ij,\mu} = k_\mu(\mathbf{d}_{ij}, \Sigma)$ as

$$(\beta_1, \ldots, \beta_i, \ldots, \beta_N)^\mathsf{T} = K_\mu^{-1}\mathbf{n}. \tag{9}$$

The contact points during the exploration could potentially be used to refine the object shape representation, but this is useful in the case that they provide radically new information, for instance, when exploring occluded parts of the object, which is clearly a point for future investigation.

Both functions $f(\mathbf{x})$ and $m(\mathbf{x})$ comprise an enhancement of the object representation w.r.t. previous approaches, such as [11] and [12], where only the shape information is used.

B. Exploration paths: Geodesic flows on implicit surfaces

Paths for exploration should have a good ratio between information gain and exploration length (time or distance). A way to achieve this is to walk in straight lines over the surface for a minimal walking distance, whence the name geodesic flows. The flow can be computed out of the geodesic curvature equation of an implicit surface and integrating from a point $(x, y, z)^(0)$ and a tangent vector $(p, q, r)^(0)$ to the surface, until the curve have a predefined length. Thus, given an implicit function $f(x, y, z)$, the geodesic curve equation can formulated in the following six first-order differential equations

$$\begin{cases} x' = & p \\ y' = & q \\ z' = & r \\ e' = & ((pf_z - rf_x)r + (pf_y - qf_x)q)L/D \\ f' = & ((qf_z - rf_y)r + (qf_x - pf_y)p)L/D \\ g' = & ((rf_y - qf_z)q + (rf_x - pf_z)p)L/D, \end{cases} \tag{10}$$

with

$$\begin{aligned} L &= f_{xx}p^2 + f_{yy}q^2 + f_{zz}r^2 + 2(f_{xy}pq + f_{yz}qr + f_{xz}pr) \\ D &= (rf_y - qf_z)(rf_y - qf_z) + (pf_z - rf_x)(pf_z - rf_x) + \\ &\qquad + (qf_x - pf_y)(qf_x - pf_y). \end{aligned}$$

The first and second order derivatives of (2) required in (10) are

$$\frac{\delta f}{\delta \mathbf{x}} = \sum_{i=1}^{N} \alpha_i \frac{\delta k_{\mathbb{R}_3}(\mathbf{d}, \sigma)}{\delta \mathbf{d}} \frac{\delta \mathbf{d}}{\delta \mathbf{x}}, \tag{11}$$

and

$$\frac{\delta^2 f}{\delta \mathbf{x}^2} = \sum_{i=1}^{N} \alpha_i \frac{\delta^2 k_{\mathbb{R}_3}(\mathbf{d}, \sigma)}{\delta \mathbf{d}^2} \frac{\delta^2 \mathbf{d}}{\delta \mathbf{x}^2}, \tag{12}$$

where

$$\frac{\delta k_{\mathbb{R}_3}}{\delta \mathbf{d}} = \begin{cases} -\dfrac{1}{2\sigma} \dfrac{\mathbf{d}^\mathsf{T}}{(\mathbf{d}^\mathsf{T}\mathbf{d})^{\frac{1}{2}}} & \text{if } (\mathbf{d}^\mathsf{T}\mathbf{d})^{\frac{1}{2}} \leq 2\sigma \\ \mathbf{0} & \text{if } (\mathbf{d}^\mathsf{T}\mathbf{d})^{\frac{1}{2}} > 2\sigma, \end{cases} \tag{13}$$

and

$$\frac{\delta^2 k_{\mathbb{R}_3}}{\delta \mathbf{d}^2} = \begin{cases} -\dfrac{1}{2\sigma} \dfrac{\mathbf{I}_3\mathbf{d}^\mathsf{T}\mathbf{d} - \mathbf{d}\mathbf{d}^\mathsf{T}}{(\mathbf{d}^\mathsf{T}\mathbf{d})^{\frac{3}{2}}} & \text{if } (\mathbf{d}^\mathsf{T}\mathbf{d})^{\frac{1}{2}} \leq 2\sigma \\ \mathbf{0}_3 & \text{if } (\mathbf{d}^\mathsf{T}\mathbf{d})^{\frac{1}{2}} > 2\sigma. \end{cases} \tag{14}$$

Thus, by integrating (10) using (2), (11), and (12), we obtain geodesic flows γ_i over the object surface, as shown in Fig. 3.

C. Contour following: Stiffness controller

The tactile data acquisition can only be successful when the contact with the object surface is guaranteed. To this end, force and trajectory control is required during the exploration. Considering that there is no exact description of the object shape, executing a pure position control might be dangerous for the equipment. The presented ITs includes a compliant structure for safety, however, when the KUKA arm uses the stiffness controller, it behaves like a spring with defined stiffness and damping parameters. In such manner, we set the parameters to make the PPCC to seem infinitely stiff. The provided control law for the arm for this mode is

$$\boldsymbol{\tau} = \mathbf{J}^\mathsf{T}(K_c(X_\text{d} - X) + \mathbf{f}_\text{d}) + B(\mathbf{d}) + \boldsymbol{\tau}_\text{dyn}, \tag{15}$$

where $X_\text{d} \in SE(3)$ is the desired tool frame, $\mathbf{f}_\text{d} \in \mathbb{R}^6$ is the desired force at the tool, $K_c \in \mathbb{R}^6$ is the desired Cartesian stiffness of the tool frame specified along the three axes, and $\mathbf{d}$ the desired damping behavior.

Concerning the contour following, the origin of the desired tool frame is taken directly from the integration of the

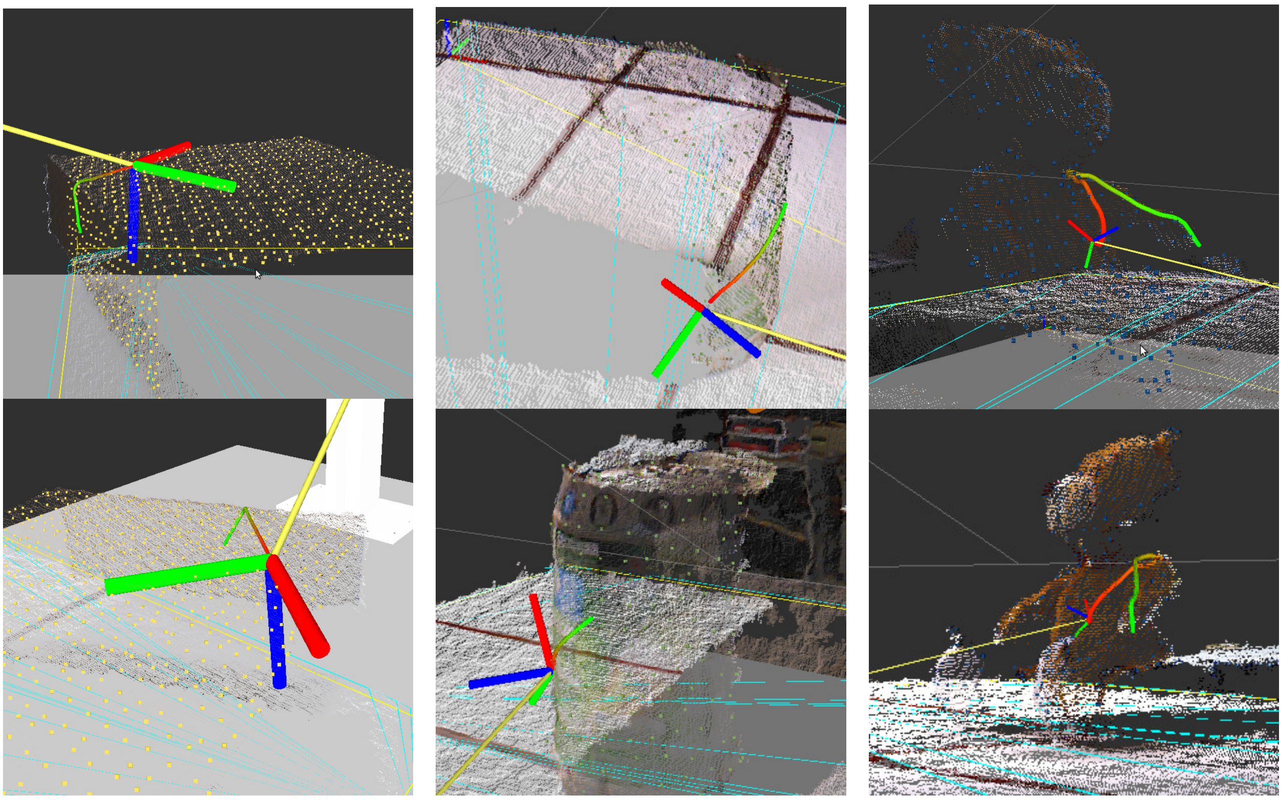

(a) The box has flat surfaces, hence geodesic flows are straight lines.

(b) The can is practically a cylinder, hence geodesic flows are elliptical curves.

(c) The teddy bear has a very irregular shape, but still geodesic flows are found.

Fig. 3: Geodesic flows on object surfaces captured by an RGB-D sensor. The color of the flow goes from red, i.e. the initial contact point, to green, i.e. the final position, according to the predefined length of the curve.

geodesic curve. The orientation, instead, is corrected to keep the $\mathbf{z}_{\mathrm{r}}$ axis of the end-effector reference frame aligned with the normal at the contact point $\mathbf{z}_{\mathrm{c}}$. This is due to the fact that the arm lacks the capability to render any desired Cartesian stiffness in this mode. Thus, since the tip of the ITs is spherical, the orientation correction is equivalent to a a fixed contact point w.r.t. to the sensor frame. The error rotation matrix can be readily obtained from angle-axis parameters, with angle

$$\theta = \cos^{-1}(\mathbf{z}_c \cdot \mathbf{z}_{\mathrm{r}}),$$

and axis

$$\mathbf{a} = \frac{\mathbf{z}_c \times \mathbf{z}_{\mathrm{r}}}{\sin(\theta)}.$$

With this, and additionally setting a lower stiff value on the $\mathbf{z}_{\mathrm{r}}$ axis of the tool, as well as a non-zero desired contact force along it, a safe contact and shape accommodation is furnished during the haptic exploration.

D. Summary: Exploration logic

The three elements from the previous subsections are looped following the pseudo-code outlined in Algorithm 1, where the arguments of implicit functions f, m are omitted for clarity. The SEGMENTOBJECT and RECORDTACTILEDATA functions are related to the data acquisition process described in Section II. Functions COMPUTESHAPE and COMPUTEFRICTION are essentially the weight computations in (7) and (9). Function COMPUTEGEODESIC is the integration of (10). The EXPLORING(γ_i) loop is performed using the contour following procedure from Section III-C. A clear point for future discussion is how to systematically break the INFORMATIONGAIN loop.

Algorithm 1: Exploration logic.

Data: Scene point cloud $\mathcal{S}$, and parameters
Result: Object representation (f, m)
$\mathcal{C}$ = SEGMENTOBJECT($\mathcal{S}$);
f = COMPUTESHAPE($\mathcal{C}$);
while INFORMATIONGAIN **do**
  $\mathbf{x}_i$ = SAMPLEPOINT(f);
  $\mathbf{t}_i$ = SAMPLEDIRECTION($f, \mathbf{x}_i$);
  γ_i = COMPUTEGEODESIC($f, \mathbf{x}_i, \mathbf{t}_i$);
  while EXPLORING(γ_i) **do**
    $(\mathbf{x}_j^{(t)}, \mathbf{f}_j^{(t)}, \mu^{(t)})$ = RECORDTACTILEDATA();
  m = COMPUTEFRICTION($\mathcal{C}, \mathbf{x}_j^{(\forall t)}, \mathbf{f}_j^{(\forall t)}, \mu^{(\forall t)}$);
return $(f(\mathbf{x}), m(\mathbf{x}))$;

IV. EXPERIMENTS

A. Implementation details

The object point cloud segmentation is done in four steps. First, we apply a pass-through filter over the complete

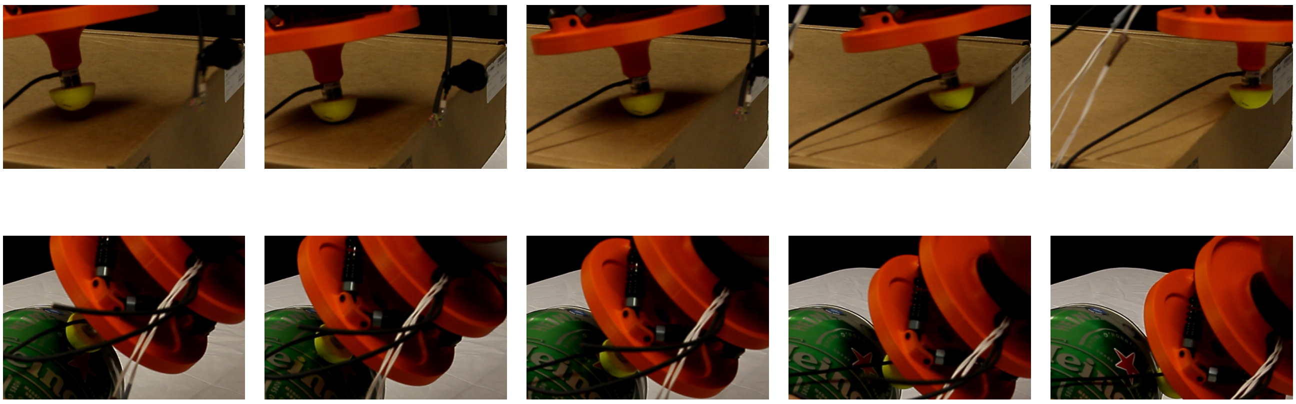

Fig. 4: Haptic exploration over objects. Top: a paperboard box. Bottom: a can.

TABLE I: Parameters used for the experiments.

Parameter	Value
RGB-D sensor, object modeling, and global trajectories	
Leaf size (downsampling)	0.02m
Min cluster size	500
Surface smoothing factor σ	100m
Friction smoothing factor Σ	5
Int. fixed-step Runge-Kutta	0.0001
Geodesic flow length	15cm
KUKA lwr, ITs, and contour following	
Robot cycle time	2ms
Cartesian stiffness $(\{\mathcal{E}\})$	$(10, 10, 2, 5, 5, 5) \cdot 10^2$[N/m, Nm/rad]
Desired force in $z_{\mathcal{E}}$	5N
Orientation correction gain	0.001
ITs force threshold	0.1N
Tip radius	0.02m
F/T filt. low-pass cutoff freq.	5Hz

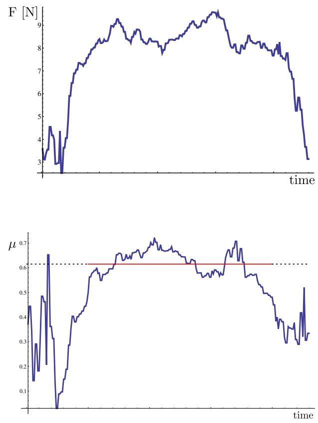

(a) Exploration over the box. Material: Paperboard.

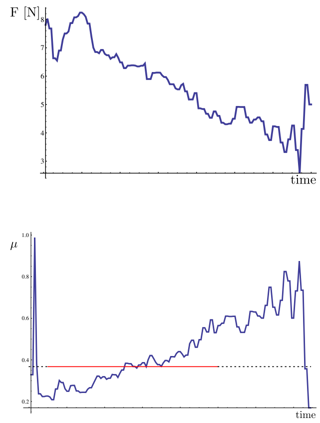

(b) Exploration over the can. Material: Aluminum.

Fig. 5: Relevant data recorded during the haptic exploration. Top: Force along $\mathbf{z}_c$ used to detect the contact and non-contact states for. Bottom: Friction coefficient μ, the red line marks the mean value during the contact state.

point cloud to keep the table and object. Then, a dominant plane is estimated using RANSAC techniques on the filtered cloud. The table is removed, so only the object point cloud remains, which is downsampled to speed up computations. This process is aided by the PointCloud library [15] and the ROS system [16]. The numerical integration of the geodesic flows is performed using the boost C++ odeint library. The F/T sensor used in the ITs is the ATI Nano17 SI-25-0.25. A low-pass filter was applied to the F/T measurements to have a smoother contact estimation. The tip and the PPCC were designed in our lab. The arm where the ITs is mounted on is the 7 DoF KUKA LWR controlled through the Standford Fast Research Interface Library (FRIL). The data acquisition and synchronization interface between the KUKA impedance controller, the RGB-D sensor and the 6-axes F/T sensor were developed in C++. The relevant parameters used for the experiments are shown in Table I.

B. Results and discussion

In Fig. 4, we show snapshots of the haptic exploration for two objects, a cardboard box and an aluminum can. The maximum distance between the planned and executed trajectories goes up to 2cm in the box, and 0.5cm in the can, caused, for instance, by the camera-robot calibration, the PPCC and object deformation, and F/T measurements. The force measured along $\mathbf{z}_c$ is used to determine the contact state of the trajectory to properly estimate the friction coefficient. Both are plotted in Fig. 5 for a single trajectory. We get a mean value of $\mu = 0.62$ and $\mu = 0.36$ for the box (ABS/Paperboard) and the can (ABS/Metal), respectively. In Fig. 6, the object shape with the friction coefficient estimation is shown after the haptic exploration along the geodesic flow. The points on the surface are obtained by sampling (2) and the color is obtained by evaluating (4), confirming that the methodology is capable of representing both visual and tactile data.

V. Conclusions

This work proposed a novel object representation and the exploration strategy to instantiate it. The added value with respect to previous approaches is the consideration of the friction coefficient within the representation. This added information is essential to relevant robotic fields such as grasp

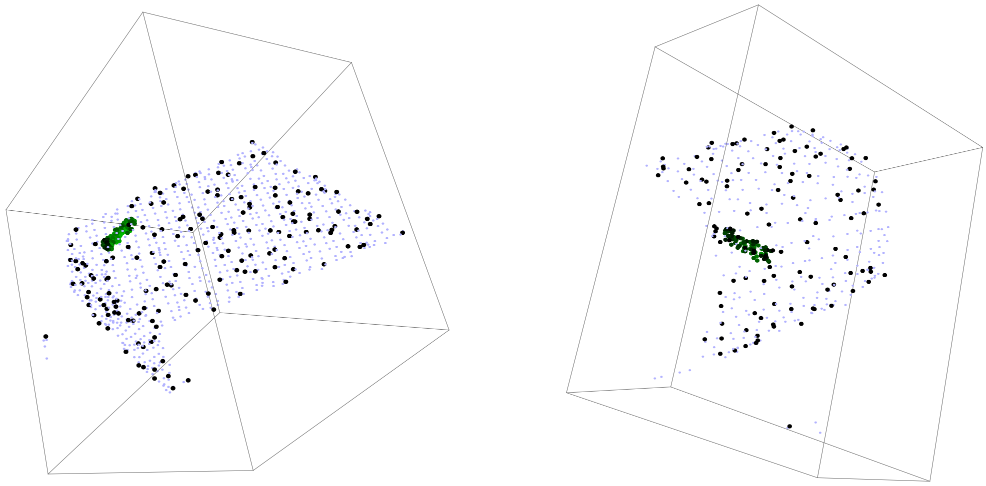

(a) Box

(b) Can

Fig. 6: Points on the object surface are colored with the estimated value of the friction coefficient, that is, the greener the higher, the darker the lower. Note that near the explored trajectory, the friction coefficient is non-zero even when the points are not exactly on the trajectory. The actual surface points are smaller and shown in light blue for clarity.

planning and manipulation using mechanical hands, and potentially useful in object recognition, in a similar way as [17] recognizes textures. Whereas the visual data was acquired using a well-known RGB-D sensor, the tactile data demanded a crude but effective Intrinsic Tactile sensor mounted on a robot's end-effector, acting as an haptic exploratory probe. The exploration is planned in minimal length paths over the object surface, i.e. geodesic flows, to looking to increase the information gain and exploration length ratio. The actual contour following used an stiffness controller for safety, and shape accommodation while ensuring a continuous contact during the exploration. The preliminary experimental results on a single-finger-like fashion revealed a valid approach to have both visual and tactile data in a single probabilistic framework using Gaussian processes.

Several points deserve further attention, such as how to generate points outside/inside the surface for a generic case, or the decision on when to end the exploration if no more information is gained, or how a different contour following controller can affect the quality of acquired data. Future work also involves the use of a dexterous hand equipped with ITs at the fingertips, to explore the limitations due to a reduced mobility, and possibly, the benefits of a parallel tactile data acquisition system.

VI. Acknowledgement

This work is supported by the grant no. 600918 "PACMAN" - Probabilistic and Compositional Representations of Object for Robotic Manipulation - within the FP7-ICT-2011-9 program "Cognitive Systems". European Research Council and under the ERC Advanced Grant no. 291166 SoftHands (A Theory of Soft Synergies for a New Generation of Artificial Hands).

The first author would like thank M. Bonilla for his support in the code implementation.

References

[1] W. E. L. Grimson and T. Lozano-Perez, "Model-Based recognition and localization from sparse range or tactile data," *The Int. J. of Rob. Res.*, vol. 3, no. 3, pp. 3–35, Sept. 1984.

[2] P. Allen and R. Bajcsy, "Robotic object recognition using vision and touch," in *Proc. of the 9th Int. Joint Conf. on Artif. Intel.*, 1987, pp. 1131–1137.

[3] J. Ilonen, J. Bohg, and V. Kyrki, "Fusing visual and tactile sensing for 3-D object reconstruction while grasping," in *Proc. of the IEEE Int. Conf. on Rob. and Aut.*, 2013, pp. 3547–3554.

[4] M. Chalon, J. Reinecke, and M. Pfanne, "Online in-hand object localization," in *Proc. of the IEEE/RSJ Int. Conf. on Intel. Rob. and Sys.*, 2013, pp. 2977–2984.

[5] R. Bajcsy, "What can we learn from one finger experiments?" in *International Symposium on Robotics Research*, 1984.

[6] P. Dario and G. Buttazzo, "An anthropomorphic robot finger for investigating artificial tactile perception," *The Int. J. of Rob. Res.*, vol. 6, no. 3, pp. 25–48, 1987.

[7] A. Bicchi, J. K. Salisbury, and D. L. Brock, "Contact sensing from force measurements," *The Int. J. of Rob. Res.*, vol. 12, no. 3, pp. 249–262, June 1993.

[8] R. Bajcsy, S. Lederman, and R. L. Klatzky, "Machine systems for exploration and manipulation a conceptual framework and method of evaluation," Tech. Rep., 1989.

[9] K. Hang, F. T. Pokorny, and D. Kragic, "Friction coefficients and grasp synthesis," in *Proc. of the IEEE/RSJ Int. Conf. on Intel. Rob. and Sys.* IEEE, Nov. 2013, pp. 3520–3526.

[10] R. Detry and J. Piater, "Continuous Surface-Point distributions for 3D object pose estimation and recognition," in *Computer Vision ACCV 2010*, ser. Lecture Notes in Computer Science, R. Kimmel, R. Klette, and A. Sugimoto, Eds., 2011, vol. 6494, ch. 45, pp. 572–585.

[11] S. Dragiev, M. Toussaint, and M. Gienger, "Gaussian process implicit surfaces for shape estimation and grasping," in *Proc. of the IEEE Int. Conf. on Rob. and Aut.*, May 2011, pp. 2845–2850.

[12] S. El-Khoury, M. Li, and A. Billard, "On the generation of a variety of grasps," *Rob. and Aut. Sys.*, vol. 61, no. 12, pp. 1335–1349, 2013.

[13] C. E. Rasmussen and C. K. I. Williams, *Gaussian Processes for Machine Learning*. The MIT Press, 2006.

[14] "NUKLEI: Kernel methods for SE(3) data (a c++ machine-learning library)," http://nuklei.sourceforge.net/.

[15] R. B. Rusu and S. Cousins, "3D is here: Point cloud library (PCL)," in *Proc. of the IEEE Int. Conf. on Rob. and Aut.*, 2011, pp. 1–4.

[16] "ROS: Robot operating system," www.ros.org.

[17] P. Dallaire, P. Giguere, D. Émond, and B. Chaib-draa, "Autonomous tactile perception: A combined improved sensing and bayesian nonparametric approach," *Rob. and Aut. Sys.*, 2014.